



HAL
open science

Flaw detection on Inconel600® using separation of single and multiple scattering contributions

Sharfine Shahjahan, Alexandre Aubry, Fabienne Rupin, Bertrand Chassignole,
Arnaud Derode

► **To cite this version:**

Sharfine Shahjahan, Alexandre Aubry, Fabienne Rupin, Bertrand Chassignole, Arnaud Derode. Flaw detection on Inconel600® using separation of single and multiple scattering contributions. *Acoustics* 2012, Apr 2012, Nantes, France. hal-00810831

HAL Id: hal-00810831

<https://hal.science/hal-00810831>

Submitted on 23 Apr 2012

HAL is a multi-disciplinary open access archive for the deposit and dissemination of scientific research documents, whether they are published or not. The documents may come from teaching and research institutions in France or abroad, or from public or private research centers.

L'archive ouverte pluridisciplinaire **HAL**, est destinée au dépôt et à la diffusion de documents scientifiques de niveau recherche, publiés ou non, émanant des établissements d'enseignement et de recherche français ou étrangers, des laboratoires publics ou privés.



ACOUSTICS 2012

Flaw detection on Inconel600® using separation of single and multiple scattering contributions

S. Shahjahan^a, A. Aubry^b, F. Rupin^a, B. Chassignole^a and A. Derode^b

^aEDF R&D, Site des Renardières, Avenue des Renardières - Ecuelle, 77818 Moret Sur Loing, France

^bInstitut Langevin, 10, rue Vauquelin, 75005 Paris, France
sharfine.shahjahan@edf.fr

Flaw detection using ultrasonic non destructive testing on coarse grain steels commonly found in nuclear power plants is disturbed by a high backscattered noise. This leads to a decrease of the detection capabilities of common ultrasonic testing techniques, particularly at high frequencies and large depths for which multiple scattering dominates. Recent studies have shown that the contribution of single scattering could be extracted from multiple scattering in complex medium. These results were obtained on a model random medium made of parallel steel rods immersed in water. They showed that the ability to detect a target could be significantly increased using a specific filtering method, based on matrix properties, in supplement with the D.O.R.T. method. In this work, this new method is now applied to real materials. Experimental results on a nickel based alloy (Inconel600®) mock-up exhibiting manufactured flaws are presented and compared to other detection techniques. The experimental set-up uses a 64-element ultrasonic array, around 3 MHz. Despite a high backscattering noise due to multiple scattering, the first results show a dramatic improvement of the detection performances.

1 Introduction

Numerous non destructive inspections in nuclear power plants are performed during monitoring operations in order to detect the potential appearance of a defect during service. Ultrasonic techniques are mostly used because of their abilities of detection and sizing. Nevertheless, detection performances decrease for materials with a coarse grain structure. Indeed, when the wavelength is comparable to the grain size, the wave is scattered at each grain boundary. As a result, multiple scattering occurs and increases the backscattered noise and the wave attenuation [1, 2].

Solutions to improve imaging in polycrystalline media are the subject of numerous studies in the literature. Spectral improvement, cross-correlation or wavelet post processing have been proposed to optimize the detection [3-6]. Synthetic focused image can also be constructed with array probes, by means of the full matrix capture (FMC) [7, 8] and proper beamforming, as commonly done for instance in medical imaging [9]. Time reversal imaging is also possible by using phased array to optimize target detection in homogeneous or weakly scattering media but remains difficult in presence of an important multiple scattering [10-16]. Recent studies on the reduction of the multiple scattering contribution have been developed on synthetic model media (forests of steel rods immersed in water) in order to improve time reversal imaging [16]. These studies, based on random matrix theory, discriminate single and multiple scattering contributions in the total backscattered signals. The technique relies on a particular property of single scattering: a deterministic coherence along the antidiagonals of the array response matrix.

The purpose of this paper is to apply this separation technique on a metallic polycrystalline sample with strong scattering. The experiments were performed on a nickel based alloy (Inconel600®) exhibiting a coarse grain microstructure in which a defect has been manufactured (Side Drilled Hole) at 70 mm depth. Section 2 describes the basic principles of the separation and detection method. Experimental results obtained on Inconel600® are presented and compared to classical imaging techniques (plane wave B-scan, total focusing method) in section 3.

2 Principles

2.1 D.O.R.T. imaging

The decomposition of the time reversal operator (D.O.R.T.) method is a technique that uses the response matrix of the medium to realize selective target detection

[11, 17]. This matrix, denoted \mathbf{K} , contains the whole available information of the inspected medium. It is acquired using a N-element array probe combined with a full matrix capture (FMC). The FMC is based on N sequences, each of which consists in emitting a pulse with one element and recording the response of the N array elements simultaneously. After repeating this sequence for every transmitting element, the N^2 signals are arranged in a matrix $\mathbf{H}(t)$. The matrix is truncated in overlapping time windows of duration T, and a short-time Fourier analysis results in a N-by-N complex matrix $\mathbf{K}(T, f)$ for each time T and frequency f. \mathbf{K} can be used for target detection with the D.O.R.T. method.

The D.O.R.T. method is based on a singular value decomposition of the array response matrix. Indeed, the \mathbf{K} matrix can be written as $\mathbf{K}=\mathbf{U}\mathbf{S}\mathbf{V}$ where \mathbf{U} and \mathbf{V} are unitary matrices containing singular vectors and \mathbf{S} is a diagonal matrix containing the singular values (labeled λ_i , with $i=1, \dots, N$) of \mathbf{K} . In the very simple case of a homogeneous medium which contains less than N point-like targets, as long as multiple scattering between targets is neglected then each target can be associated to a singular value and a singular vector [17]. Basically, the singular value λ_i is proportional to the reflectivity of the i-th target, and the corresponding singular vector gives the set of amplitudes and delays (phase shifts, in the frequency domain) that must be applied to the array elements in order to focus selectively on that precise target. The image of the i-th target is obtained by $I_i(T, f)=\lambda_i|\mathbf{V}_i(T, f)\mathbf{G}^*(T, f)|$ where \mathbf{G} is the matrix associated to the Green function of the homogeneous medium.

As efficient as this method can be in a homogeneous or weakly scattering materials [12, 17], it is limited when multiple scattering occurs. Indeed when the structural noise dominates, the eigenspace associated to the non-zero singular values is no more linked to the direct echoes coming from the point-like targets, but can be related to the structural noise. The problem is to separate the “signal sub-space” of interest (the echoes from the targets to be imaged) from the noise sub-space (the structural grain noise, which may include multiple scattering contributions). In the following, this will be referred to as “filtering” the multiple scattering contribution.

2.2 Filtering multiple scattering

The matrix \mathbf{K} has to be “filtered” in order to reduce the multiple scattering contribution before imaging [15, 16].

$\mathbf{K}(T, f)$ is the sum of all wave contributions that arrive at the receivers in the time-window $[t-T/2; t+T/2]$, at the frequency f. In the general case, it contains both single scattering (SS) and multiple scattering (MS) contributions:

$\mathbf{K}=\mathbf{K}^{SS}+\mathbf{K}^{MS}$. If we imagine a target as a hole in a scattering structure, the direct echo from the target is somewhere in \mathbf{K}^{SS} , while the structural grain noise is partly in \mathbf{K}^{SS} , partly in \mathbf{K}^{MS} . For imaging purposes, one tries to eliminate \mathbf{K}^{MS} as much as possible.

Aubry et al. have shown two typical behaviors when either SS or MS dominates [18]. When MS dominates, \mathbf{K} was found to be similar to a classical random matrix, whereas when SS dominates \mathbf{K} is similar to a Hankel's matrix. This has two consequences. Firstly, the distribution of the singular values, $\rho(\lambda)$ is not the same in the MS and in the SS regimes. Secondly, in the SS regime, the coefficients k_{ab} of the \mathbf{K} matrix verify the following property: whatever the realization of disorder, there is a deterministic phase relation between coefficients of \mathbf{K} belonging to the same antidiagonal, i.e., couples of transmitters (a) and receivers (b) such that $a+b$ is a constant. This relation is:

$$\beta_m = \frac{k_{a-m, a+m}}{k_{aa}} = \exp\left(\frac{j2\pi(mp)^2}{\lambda R}\right) \quad (1)$$

with $mp=(x_a-x_b)/2$, x_a and x_b are respectively the position of the emitter and of the receiver, $R=cT/2$ and p is the pitch of the array.

Eq (1) implies that whatever the medium, as long as there is only single scattering ($\mathbf{K}^{MS}=0$) the elements of \mathbf{K} have a long-range deterministic coherence along their antidiagonals. On the contrary, when $\mathbf{K}^{SS}=0$ and multiple scattering dominates, there is no such coherence. This is the key to separate single and multiple scattering contributions. The details of the method are explained in [15, 18].

By and large, the idea consists of a three-step process: the total matrix $\mathbf{K}=\mathbf{K}^{SS}+\mathbf{K}^{MS}$ is rotated by 45° into a new matrix \mathbf{A} whose columns correspond to the antidiagonals of \mathbf{K} . \mathbf{A} is projected along the vector defined by Eq. (1), which amounts to extracting from the total matrix the part that exhibits the particular form of coherence which is typical of single scattering. Finally, the "filtered" version of \mathbf{A} is rotated back by -45° . Ideally, the resulting matrix \mathbf{K}^F should be devoid of multiple scattering: $\mathbf{K}^F \approx \mathbf{K}^{SS}$. Naturally this is only an approximation [15, 16], but the aim of this study is to test the basic concept on a strongly scattering material such as a polycrystalline metal containing a flaw.

2.3 Detection criterion

The target detection consists in performing a singular value decomposition (SVD) of the array response matrix \mathbf{K} , and then determine whether the strongest of its singular value λ_1 is associated to a target (here a flaw in the structure) or if it is associated to structural noise. The general principles of the method have already been published elsewhere [15, 16, 18]. Briefly, in order to determine a detection criterion, the cumulative distribution function F_1 of the random variable λ_1 has to be known. In ideal cases (purely single-scattering medium, purely multiple scattering medium, $N \rightarrow \infty$), analytic expressions can be derived from random matrix theory. In a real experiment, single scattering and multiple scattering coexist, and there is usually no analytic expression for F_1 . So instead, F_1 is first determined by probing a zone of the medium free of any defect. By building the cumulative histogram of the first singular value, we obtain an estimator of the distribution function F_1 , which is plotted in figure 6.

Once F_1 is known in the flawless area, it is used to establish a detection criterion. To that end, the operator fixes an acceptable probability of false alarm (PFA), say 1%. This defines a threshold α such that $F_1(\alpha)=1-PFA$.

Next, the array is placed in a zone where there might be a defect. The matrices $\mathbf{K}(T,f)$ are recorded. They are "filtered" in order to eliminate multiple scattering, which yields another set of matrices $\mathbf{K}^F(T,f)$. A SVD is performed (at each time T and frequency f), and the strongest singular value is compared to the threshold. If $\lambda_1(T,f) > \alpha(T,f)$, the operator detects a defect, with a probability of $F_1(\lambda_1)$. And in order to build an image of the medium, the D.O.R.T. method is applied: the singular vector corresponding to λ_1 is back-propagated, as explained in paragraph 2.1, as if the medium was homogeneous with a constant velocity c .

In the next section, we apply this method to an Inconel600® sample ($c=5850\text{m/s}$) and compare it to other classical techniques.

3 Experimental results

3.1 Experimental setup

The inspected medium is a block referenced B4 made of Inconel600® which is a nickel-based alloy commonly used in the nuclear industry. This block was harvested from a forged bar and underwent a specific heat treatment to induce a growth of the mean grain size. A metallographic analysis performed on a $17 \times 13\text{mm}^2$ sample of the mock-up leads to an estimation of the mean grain size of $750\mu\text{m}$. This medium is considered to be highly scattering around 3 MHz [19] and contains a side drilled hole of radius $r=1\text{mm}$ and localized at 70mm depth. A second mock-up referenced B1, made of Inconel600 with a mean grain size estimated to $90\mu\text{m}$ with a side drilled hole at 70mm depth is used as a reference. This second mock-up is considered to be weakly scattering around 3 MHz [19].

The array probe is a 64-element linear array (central frequency $F_c=3\text{MHz}$). The element size is $0.39 \times 12\text{mm}^2$ with an array pitch of 0.417 mm and the sampling frequency is 40 MHz. The blocks are immersed in a water tank and the probe is in contact configuration (figure 1).

The reference data are obtained on the 4 faces of the block in an area free from any defect. On each face, 30 different acquisitions are performed. Finally, 120 full matrix responses $\mathbf{H}(t)$ are recorded.

Then, the acquisitions of $\mathbf{H}(t)$ in presence of a defect are realized at 11 different probe positions recorded along the cylindrical flaw (y axis in figure 1).

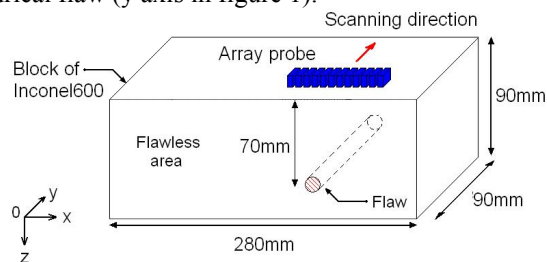


Figure 1: Illustration of the experimental setup.

3.2 Synthetic imaging

Once the matrix $\mathbf{H}(t)$ is acquired, classical post-treatment can be realized by summation and time shift operations on the $h_{ij}(t)$ signals in order to create a synthetic image of the medium [7, 9].

Firstly, adjacent elements responses are added to create a plane wave response with an aperture of M elements as described by Eq. (2).

$$I(x = pm, z = ct) = \left| \sum_{i=m}^{m+M-1} \sum_{j=m}^{m+M-1} h_{ij}(t) \right| \quad (2)$$

Where p is the pitch size and c is the longitudinal velocity. Figure 2 shows the resulting image for one realization, with $M=4$ adjacent elements: the flaw is not detected for block B4 while it is clearly detected for block B1. The other 11 acquisitions confirm that this technique is not able to detect the side drilled hole on block B4.

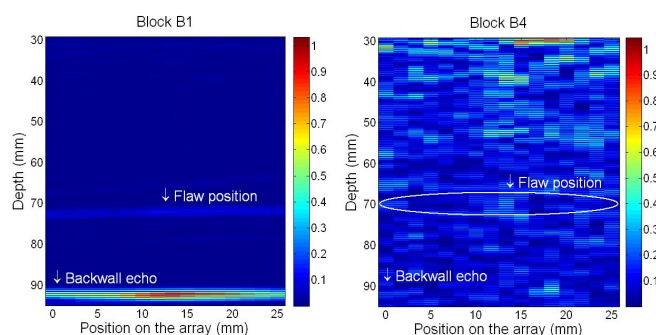


Figure 2: Plane wave B-scan image of one acquisition constructed by using 4 adjacent elements for block B1 (left) and block B4 (right).

An other possible technique consists in calculating the synthetic images for each acquisition using the total focusing method (TFM). The signals from all the elements in the array are summed to synthesize a focus at every point (x,z) of the inspected zone as Eq. (3).

$$I(x, z = ct) = \left| \sum_{i,j} h_{ij} \left(\frac{\sqrt{(x_i - x)^2 + z^2} + \sqrt{(x_j - x)^2 + z^2}}{c} \right) \right| \quad (3)$$

Where z is related to the propagation time by $z=ct$.

Figure 3 shows one computed image for each block: the flaw is detected for block B1 whereas for block B4 the noise level is important so that the side drilled hole is difficult to detect.

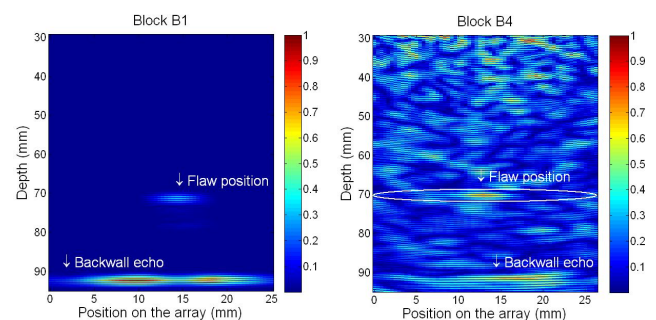


Figure 3: Total focusing method image of block B1 (left) and block B4 (right) for one position.

3.3 Target detection

The 120 acquisitions of the matrix $\mathbf{H}(t)$ in the flawless area of the medium provide, for each time T and frequency f , a set of 120 independent realizations which are used to estimate the probability density function ρ for the singular values λ . Figure 4 displays the resulting estimate $\hat{\rho}(\lambda)$, at $f=3.8\text{MHz}$ and shows that the distribution is not too far from the quarter circle law [15]. It confirms that for this frequency \mathbf{K} behaves almost like a classical random matrix.

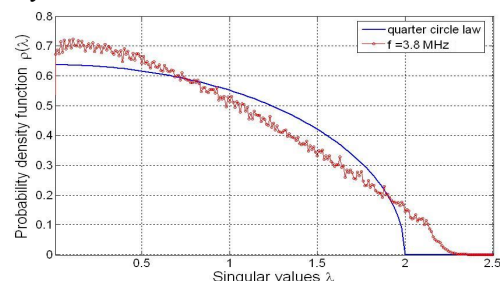


Figure 4: Estimate of the probability density function of λ at 3.8MHz and between 15 and 29 μs . The quarter circle law is plotted for comparison purpose.

After filtering, the estimate for the distribution ρ^F at $f=3.8\text{MHz}$ is closer to that of Hankel matrices [15] (figure 5). It indicates that the filtering is efficient and leads to a distribution of singular values closer to what is expected for single scattering.

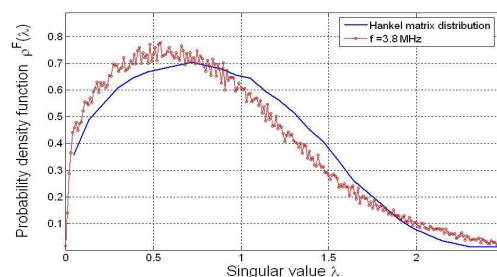


Figure 5: Estimate of the probability density function of λ for 3.8MHz and between 15 and 29 μs , after filtering of the multiple scattering contribution. Hankel's law is plotted for comparison purpose.

Then the 120 realizations of λ_1 (the highest of singular values) are used to estimate its probability density function ρ_1 . The obtained estimator $\hat{\rho}_1$ is integrated to provide \hat{F}_1 , an estimate of the cumulative distribution function F_1 . The probability of false alarm (PFA) is set at 1%. Therefore the detection threshold α is determined by the condition $F_1(\alpha)=0.99$. Figure 6 shows an example of \hat{F}_1 with the corresponding thresholds α and α^F respectively before and after “filtering” the multiple scattering contribution. Note that the thresholds $\alpha(T,f)$ and $\alpha^F(T,f)$ are calculated for each time T and frequency f from \mathbf{K} and \mathbf{K}^F respectively.

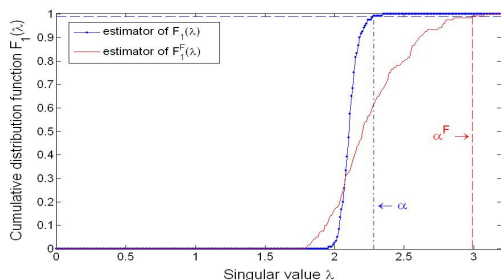


Figure 6: Example of the estimated cumulative distribution functions \hat{F}_1 and \hat{F}_1^F with their thresholds (here $z=70\text{mm}$, $f=3.8\text{MHz}$).

The D.O.R.T. method was then applied to \mathbf{K} and \mathbf{K}^F obtained in the area where the side drilled hole was located, in the most scattering block (B4).

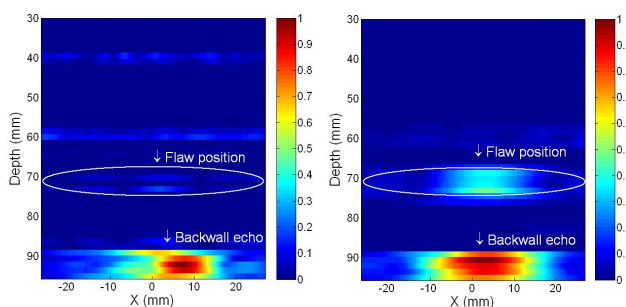


Figure 7: Example of images obtained on sample B4 with the D.O.R.T. method applied on \mathbf{K} (left) and on \mathbf{K}^F (right),

Figure 7 undoubtedly shows the effect of the « filtering » procedure, which is supposed to eliminate multiple scattering. In the image obtained from the classical D.O.R.T. method, the defect is hardly detectible (as was the case for the first two techniques), and its echo is weaker than some of the false alarms. On the contrary, the echo of the side drilled hole (SDH) is clearly visible once the « multiple scattering filter » is applied. Nevertheless some false alarms echoes appear which is not surprising since the PFA cannot be set to 0.

In order to calculate a detection rate and to evaluate the performances of the advanced focalized imaging (TFM, classical D.O.R.T., D.O.R.T. with filtering) a « signal to noise ratio », SNR, is defined as Eq. (4). It is calculated for each realization as the ratio of A_{\max} , the maximum amplitude in the flaw area for a given realization, to N_{\max} , the maximum noise for the same realization in a time window corresponding to depth between 60-80mm (see figure 8). The side drilled hole is considered to be detectible if $\text{SNR} \geq 3\text{dB}$.

$$\text{SNR}^X = 20 \log \left[\frac{A_{\max}^X}{N_{\max}^X} \right] \quad (4)$$

Here the superscript X represents the technique used (TFM image, the D.O.R.T. method on \mathbf{K} and \mathbf{K}^F).

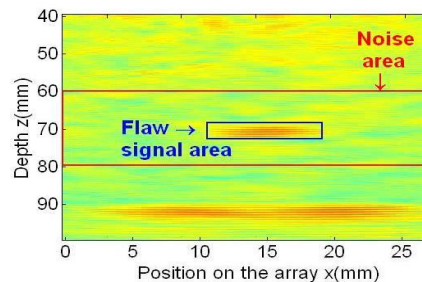


Figure 8: Example of the zone inspected in order to define the « signal-to-noise ratio ».

Table 1 summarizes the mean SNR values for each technique. The detection rates were evaluated on the ensemble of 11 positions along the same defect. The results show a clear improvement of the detection rate by using the combination of DORT method and MS filtering. Indeed, compared to TFM an improvement of 10% is observed with the classical DORT and 30% by combining with the filtering of MS. Moreover, the mean SNR is increased by 6dB and 8.5dB with DORT method respectively on \mathbf{K} and on \mathbf{K}^F . Note that in the case of DORT method the noise corresponds to the false alarms. The detection threshold was reached for the SDH for all the realizations but, in some cases, the defects were considered as not detected because of the presence of false alarms.

Table 1: Detection rate evaluated on 11 positions of the same side drilled hole for the block B4

Imaging technique	TFM	DORT with \mathbf{K}	DORT with \mathbf{K}^F
Detection rate (%)	54.5	63.6	81.8
$\langle \text{SNR} \rangle^*$ (dB)	4.0 ± 0.6	10.9 ± 4.3	12.5 ± 3.2

* averaged for realizations with $\text{SNR} \geq 3\text{dB}$.

5 Conclusion and perspectives

In this study, experiments were carried out on a block of Inconel600® in which multiple scattering occurs. In block B4, classical imaging techniques are not adapted for imaging a side drilled hole of 1 mm radius at 70mm depth. In particular, the total focusing method was not able to distinguish the flaw from noise for each acquisition. The improvement of flaw detection by reducing the multiple scattering contribution has been investigated. The combination of a filtering and a target detection method led to a reduction of the microstructural noise and consequently to an improvement of the defect detection. The first results are encouraging: an increase of detection from 54% to 82% and an improvement of 8.5dB for the SNR compared to total focusing method was observed. Nevertheless, some false alarms were produced.

The present results must be completed by the study of the influence of the microstructure (grain size, etc.). In particular, it is necessary to evaluate the limitation of the technique and to better understand the appearance of false alarms.

To do so, new experimental tests as well as numerical simulation studies will be used to perform parametrical studies (flaw size, depths, frequencies, mean grain size influence, etc.) in order to evaluate precisely the validity domain of the described method.

Acknowledgments

A. Derode is grateful for funding provided by EDF R&D, as well as the Agence Nationale de la Recherche (ANR-11-BS09-007-01) and the *pôle de compétitivité Systematic* (Research Project DiAMAN, 2012-2015).

References

1. Turner, J.A. and R.L. Weaver, *Time dependence of multiply scattered diffuse ultrasound in polycrystalline media*. Journal of the Acoustical Society of America, 1995. **97**(5): p. 2639-2644.
2. Turner, J.A., et al., *Radiative transfer and multiple scattering of diffuse ultrasound in polycrystalline media*. Journal of the Acoustical Society of America, 1994. **96**(6): p. 3675-3683.
3. Abbate, A., et al., *Signal detection and noise suppression using a wavelet transform signal processor: application to ultrasonic flaw detection*. Ultrasonics, Ferroelectrics and Frequency Control, IEEE Transactions on, 1997. **44**(1): p. 14-26.
4. Chen, J., Y. Shi, and S. Shi, *Noise analysis of digital ultrasonic system and elimination of pulse noise*. International journal of pressure vessels and piping, 1998. **75**(12): p. 887-890.
5. Chen, Y., Y. Shi, and Y. Lei, *Use of a Wavelet Analysis Technique for the Enhancement of Signal-to-noise Ratio in Ultrasonic NDE*. Insight, 1996. **38**(11): p. 800-803.
6. Yue, L. and Y. Chong-Fu, *Two signal processing techniques for the enhancement of the flaw-to-grain echo ratio*. Ultrasonics, 1987. **25**(2): p. 90-94.
7. Holmes, C., B.W. Drinkwater, and P.D. Wilcox, *Post-processing of the full matrix of ultrasonic transmit-receive array data for non-destructive evaluation*. NDT & E International, 2005. **38**(8): p. 701-711.
8. Zhang, J., et al., *Defect detection using ultrasonic arrays: The multi-mode total focusing method*. NDT & E International, 2010. **43**(2): p. 123-133.
9. Angelsen, B., *Ultrasound imaging. Waves, signals and signal processing*. Emantec. 2000, Trondheim, Norway.
10. Fink, M., et al., *Time-reversed acoustics*. Reports on Progress in Physics, 2000. **63**: p. 1933.
11. Prada, C., et al., *Time reversal techniques in ultrasonic nondestructive testing of scattering media*. Inverse Problems, 2002. **18**: p. 1761.
12. Prada, C., M. Tanter, and M. Fink. *Flaw detection in solid with the DORT method*. 1997: IEEE.
13. Kerbrat, E., et al., *Imaging in the presence of grain noise using the decomposition of the time reversal operator*. The Journal of the Acoustical Society of America, 2003. **113**: p. 1230.
14. Roux, P., et al., *Acoustical imaging through a multiple scattering medium using a time-reversal mirror*. Journal of the Acoustical Society of America, 2000. **107**(2): p. L7-L12.
15. Aubry, A. and A. Derode, *Random Matrix Theory Applied to Acoustic Backscattering and Imaging In Complex Media*. Physical review letters, 2009. **102**(8): p. 84301.
16. Aubry, A. and A. Derode, *Detection and imaging in a random medium: A matrix method to overcome multiple scattering and aberration*. Journal of Applied Physics, 2009. **106**(4): p. 044903.
17. Prada, C., et al., *Decomposition of the time reversal operator: Detection and selective focusing on two scatterers*. The Journal of the Acoustical Society of America, 1996. **99**: p. 2067.
18. Aubry, A. and A. Derode, *Singular value distribution of the propagation matrix in random scattering media*. Waves in Random and Complex Media, 2010. **20**(3): p. 333-363.
19. Shahjahan, S., et al. *Structural noise and coherent backscattering modeled with the ATHENA 2D finite elements code*. in *Acoustics 2012*. 2012. Nantes, France.